Available online at www.sciencedirect.com
ScienceDirect
Finite Elements in Analysis and Design 42 (2006) 1314–1323
FINITE ELEMENTS IN ANALYSIS AND DESIGN
www.elsevier.com/locate/finel

A hybrid-Trefftz element containing an elliptic hole

Manicka Dhanasekar[a,*], Jianjun Han[a], Qinghua Qin[b]

[a]*Centre for Railway Engineering, Central Queensland University, Building 70, Rockhampton Campus, Rockhampton, QLD 4702, Australia*
[b]*Department of Engineering, The Australian National University, Canberra, ACT 0200, Australia*

Received 21 August 2005; accepted 18 June 2006
Available online 4 August 2006

Abstract

Much work on special elements that simplify geometrical modelling of structures containing holes, cracks and/ or inclusions has been reported extensively in the literature. This paper presents a hybrid-Trefftz element containing elliptic hole formulated using Hellinger–Reissner principle by employing trial functions based on the mapping technique and the Cauchy integral method. The element presented in this paper could be regarded as an improved formulation over Piltner [Special finite elements with holes and internal cracks, Int. J. Numer. Methods Eng. 21 (1985) 1471–1485] element because the chosen trail functions in this paper have provided relatively more stable solutions. The use of the element with other ordinary displacement-based finite elements has also yielded very accurate solutions even when very coarse meshes relative to the size of the elliptic hole have been used.

Keywords: Hybrid-Trefftz finite element; Elliptic hole; Complex variable; Mapping function; Cauchy integral

1. Introduction

Structural components containing cracks, voids, inclusions, or other defects, are usually analysed using very complex, fine mesh especially around the defects in the conventional finite element analysis. To effectively describe singularity of stress fields at the crack-tip, commercial finite element programs provide singular elements formulated by collapsing rectangular elements into triangular shape for 2D analysis and rectangular prism elements into triangular pyramid shape for 3D analysis. Depending on the anticipated state of stress singularity around the crack-tip, mid-side nodes in the collapsed elements could either be moved to the quarter point position closer to the crack-tip or left unchanged in their original location.

With the objective of making the meshing simpler especially around the crack or other defects, several special elements that contain at least a single defect have been formulated and presented widely in the literature [1–12]. A comprehensive review of all these contributions is beyond the scope of this paper; only a few selected papers are reviewed here.

Using the variational principle, complex variable technique, and mapping function Tong [1] formulated several superelements based on hybrid element technique. As the stress singularity at the crack-tip has been included in the formulation of these elements, the stress intensity factors were reported directly from the nodal displacements, thus eliminating the use of any weak forms such as the J-integrals for this purpose.

Karihaloo and Xiao [2] have improved the superelements formulated in [1] by using the modified Hellinger–Reissner principle and hybrid element technique. The element was proved to efficiently determine the coefficients of higher order terms of the elastic crack-tip asymptotic fields that are important for the evaluation of the crack behaviour of elasto-plastic structures in addition to the SIF. It was shown that the results converge rapidly with *p*-refinement of the improved hybrid crack element and the *h*-refinement of the remaining regular elements.

Zeng et al. [3] also extended the work of Tong [1] to the case in which the crack faces were subjected to pressure loading using a simpler formulation without mapping function. They also presented a hybrid element containing an internal crack by statically condensing two of the crack-tip elements. Interaction between macrocrack tip and microcracks has been examined using this extended formulation.

* Corresponding author. Tel.: +61 7 4930 9677; fax: +61 7 4930 6984.
E-mail address: m.dhanasekar@cqu.edu.au (M. Dhanasekar).

0168-874X/$ - see front matter © 2006 Elsevier B.V. All rights reserved.
doi:10.1016/j.finel.2006.06.008

Piltner [4] presented a classical paper on special elements containing holes (circular and elliptical) and internal cracks. The importance of this contribution could also be inferred by reviewing the discussion of Piltner [5] on another paper that provided an element with central circular hole. Variational principles were used for the formulation of ordinary displacement and hybrid finite elements. Similar to T-complete functions (those functions that satisfy the problem domain differential equations exactly and the element boundary conditions approximately) used in the Trefftz finite element formulation, trial functions were used by Piltner [6] in the formulation of the special elements containing holes and cracks. These trial functions were chosen in such a way that the internal problem domain and local boundary conditions (for example, traction free conditions at the surface of holes) were satisfied as a priori. Formulation of eight and 16 nodded special elements containing elliptic holes and their stiffness matrices and load vectors were provided explicitly. Methods of construction of special trial functions for circular and elliptic holes were provided. The trial functions were typically chosen as a complex Laurent power series, which become sensitive when the exponent was set as a large number. Examples are provided in the paper (Section 3) that illustrates the sensitivity of Piltner elements to higher order terms. The hybrid-Trefftz element provided in this paper was also formulated similar to that of the Piltner [4] approach, but with a different trial function that exhibits good convergence characteristics with the increase in the number of series terms of trial function.

Method of constructing trial functions for the indirect types of Trefftz finite element formulation has been provided in detail by Kolodziej and Uscilowska [13]. A list of trial functions that describe the problem domain and local boundary conditions exactly has been provided in the paper and the efficiency of those functions was illustrated through three Trefftz procedures, namely the collocation, least square and Galerkin approaches. Similar contribution has been provided by Piltner [6]. More detailed description of Trefftz finite element is widely available in recent literature and some introduction to this method could be found in [9,14].

Freitas and Ji [15] presented an element model for crack problems based on fundamental conditions of equilibrium, compatibility and elasticity without associating energy equations. Their model did not include a distinct node set and as a consequence was not regarded as a superelement similar to that of Tong et al. [1]. Their model, however, was regarded as a hybrid-Trefftz finite element formulation because the local singular stress field was enforced accurately whilst the inter element compatibility was only approximately satisfied through selected functions. It was shown that reasonable results were obtained using coarse meshing using this element.

Special elements with other defects were then constructed. Zhang and Katsube presented an n-sided polygonal hybrid element with a rigid circle inclusion in [10] and the same element with an elastic circle inclusion in [11]. Using the elements they studied stress concentration in heterogeneous materials with randomly dispersed inclusions. Special 3D hybrid stress elements with traction free conditions on one face was developed by Tian et al. [12]; this element might not, however, reduce the complexity of meshing like the other special elements reviewed in this section.

The aim of this paper is to provide a method for the formulation of hybrid-Trefftz element containing an elliptic hole by employing the mapping technique and the Cauchy integral method. New trial functions that provide accurate solutions, and stable results for high-order series terms, are derived. Several numerical examples of problems subjected to direct tensile stress field as well as complex bending stress field are provided to illustrate the robustness of the element presented in this paper. The formulation is implemented into the ABAQUS finite element package as a user-defined element.

2. Formulation

Consider a plane element containing an elliptic hole as shown in Fig. 1. The element domain Ω is bounded by boundaries C_s and C_u, and the boundary displacement $\tilde{u}_i$ is prescribed along C_u, and external force $\tilde{t}_i$ is prescribed along C_s. Following the Hellinger–Reissner variational principle in the absence of body force, one can define the hybrid variational functional function Π as [1]

$$\Pi = \int_{C_u} (\tilde{u}_i - u_i) t_i \, \mathrm{d}s - \int_{C_s} u_i \tilde{t}_i \, \mathrm{d}s + \frac{1}{2} \int_{\Omega} [\sigma_{ij}(u_{i,j} + u_{j,i}) - S_{ijkl}\sigma_{ij}\sigma_{kl}] \, \mathrm{d}\Omega, \tag{1}$$

where u_i, t_i, σ_{ij} and S_{ijkl} denote the displacement, traction, stress and the compliance coefficients. $\tilde{u}_i$ is the same for two adjacent elements over the common boundaries. Eq. (1) can be alternatively expressed in the constitutive and equilibrium equations as shown in the following equations within the element.

$$\tfrac{1}{2}(u_{i,j} + u_{j,i}) = S_{ijkl}\sigma_{kl}, \tag{2}$$

$$\sigma_{ij,j} = 0. \tag{3}$$

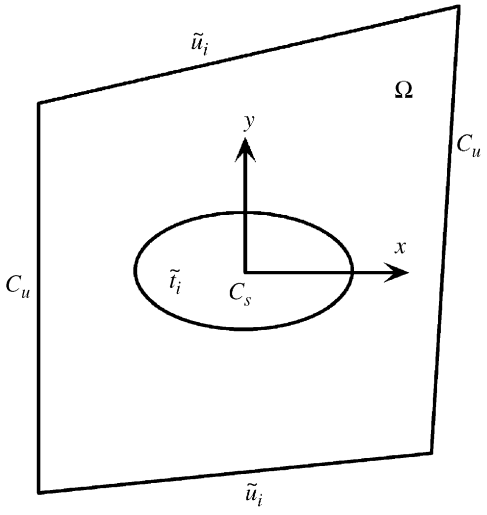

Fig. 1. A finite element with an elliptic hole subjected to displacement and stress boundary conditions.

The external force boundary condition along boundary C_s and the displacement boundary condition along boundary C_u are

$$t_i = \tilde{t}_i, \tag{4}$$

$$u_i = \tilde{u}_i. \tag{5}$$

Constructing the elliptic-hole element is to calculate the element matrix from the functional (1) by assuming u_i, σ_{ij} and $\tilde{u}_i$ in terms of proper generalised co-ordinates and interpolation functions. These four quantities can be assumed as independent of each other. However, if they are chosen in such a way that some of the Euler equations are satisfied exactly, the calculation process of the element matrix will become much easier.

For the elliptic-hole element, if the approximating functions for stress and displacement satisfy (2), (3) and the traction-free condition along C_s, the hybrid variational functional in (1) can be expressed in terms of boundary displacement, stresses and displacement in domain as

$$\Pi = \int_{C_u} \tilde{u}_i \sigma_{ij} v_j \, \mathrm{d}s - \frac{1}{2} \int_{C_u} u_i \sigma_{ij} v_j \, \mathrm{d}s \tag{6}$$

or in matrix form,

$$\Pi = \int_{C_u} \mathbf{t}^{\mathrm{T}} \tilde{\mathbf{u}} \, \mathrm{d}s - \frac{1}{2} \int_{C_u} \mathbf{t}^{\mathrm{T}} \mathbf{u} \, \mathrm{d}s \tag{7}$$

in which

$$t = \begin{bmatrix} t_1 \\ t_2 \end{bmatrix} = \begin{bmatrix} \sigma_{xx} v_x + \sigma_{xy} v_y \\ \sigma_{xy} v_x + \sigma_{yy} v_y \end{bmatrix}, \quad \mathbf{u} = \begin{bmatrix} u_1 \\ u_2 \end{bmatrix},$$
$$\tilde{\mathbf{u}} = \begin{bmatrix} \tilde{u}_1 \\ \tilde{u}_2 \end{bmatrix}. \tag{8}$$

It can be seen from Eq. (7) that only line integration along the displacement boundary C_u is required to be evaluated, which makes the calculation of the element matrix much simpler.

2.1. Element stiffness matrix

We assume that the stress and displacement approximating functions in term of generalised co-ordinates β (will be derived in the next section) are known. One can express displacement in a matrix form

$$\mathbf{u} = \mathbf{U}\beta \tag{9}$$

and by substituting the stress approximating function into Eq. (8), the boundary traction is expressed as

$$\mathbf{t} = \mathbf{R}\beta. \tag{10}$$

The boundary displacement $\tilde{\mathbf{u}}$ along C_u is separately assumed as follows:

$$\tilde{\mathbf{u}} = \mathbf{L}\mathbf{q}, \tag{11}$$

where $\mathbf{L}$ denotes the interpolation matrix relating the boundary displacement to the node displacement vector $\mathbf{q}$.

Substitution of Eqs. (9)–(11) into Eq. (7), the functional is re-expressed in terms of generalised co-ordinates and node displacements

$$\Pi = \beta^{\mathrm{T}} \mathbf{G}\mathbf{q} - \tfrac{1}{2} \beta^{\mathrm{T}} \mathbf{H} \beta, \tag{12}$$

where

$$\mathbf{G} = \int_{C_u} \mathbf{R}^{\mathrm{T}} \mathbf{L} \, \mathrm{d}s, \tag{13}$$

$$\mathbf{H} = \frac{1}{2} \int_{C_u} (\mathbf{R}^{\mathrm{T}} \mathbf{U} + \mathbf{U}^{\mathrm{T}} \mathbf{R}) \, \mathrm{d}s. \tag{14}$$

The stationary value of Π in Eq. (12) with respect to β yields the following relation:

$$\beta = \mathbf{H}^{-1} \mathbf{G}\mathbf{q}. \tag{15}$$

Substituting Eq. (15) into Eq. (12), one obtains

$$\Pi = \tfrac{1}{2} \mathbf{q}^{\mathrm{T}} \mathbf{k} \mathbf{q}, \tag{16}$$

where

$$\mathbf{k} = \mathbf{G}^{\mathrm{T}} \mathbf{H}^{-1} \mathbf{G} \tag{17}$$

is the element stiffness matrix for the elliptic-hole element.

2.2. Trial function construction

In this section, we will show the process of constructing trial functions for stress and displacement, which satisfy the constitutive, equilibrium equations and external force boundary conditions.

Employing the complex potentials $\varphi(z)$ and $\psi(z)$ [16], the stress and displacement are given as

$$\sigma_{xx} + \sigma_{yy} = 2[\Phi(z) + \overline{\Phi(z)}],$$
$$\sigma_{yy} - \sigma_{xx} + 2\mathrm{i}\tau_{xy} = 2[\bar{z}\Phi'(z) + \Psi(z)], \tag{18}$$

$$2G(u_x + \mathrm{i}u_y) = \kappa\phi(z) - z\overline{\Phi(z)} - \psi(z), \tag{19}$$

where the over bar represents the conjugate of the complex function; and $\Phi(z)=\phi'(z)$, $\Psi(z)=\psi'(z)$, and $\kappa=(3-\nu)/(1+\nu)$ for plane stress, $\kappa = 3 - 4\nu$ for plane strain, in which ν and G are Poisson's ratio and the shear modulus of the material, respectively. For any set of complex potentials $\varphi(z)$ and $\psi(z)$, the stress and displacement satisfy the constitutive and the equivalent equations within the elliptic-hole element. We have to seek for a set of potential functions to meet the traction-free condition along the boundary of the elliptic hole.

To construct the complex potential functions, we can decompose each of the two functions $\varphi(z)$ and $\psi(z)$ into two parts: a primary part and a complementary part as

$$\phi(z) = \phi_{\mathrm{p}}(z) + \phi_{\mathrm{c}}(z),$$
$$\psi(z) = \psi_{\mathrm{p}}(z) + \psi_{\mathrm{c}}(z). \tag{20}$$

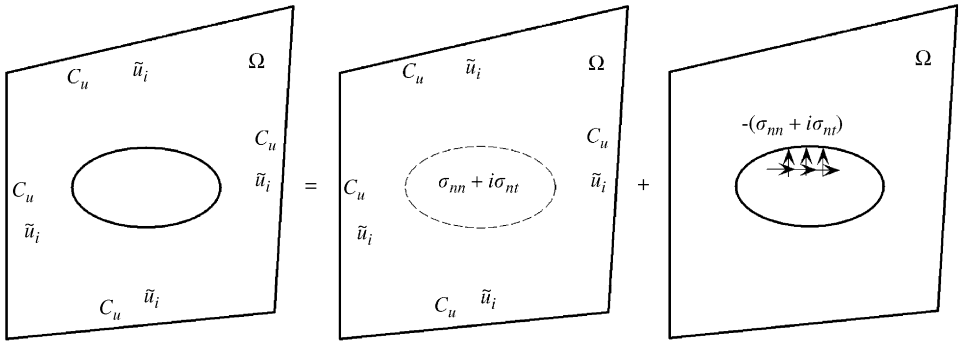

Fig. 2. Primary and complementary parts of the elliptic-hole element.

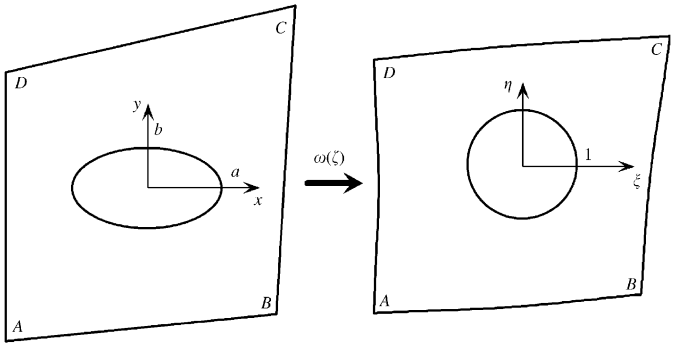

Fig. 3. Element geometries in the z and the ζ planes ($\zeta = \xi + \mathrm{i}\eta$).

The primary part corresponds to the element without the elliptic hole as shown in Fig. 2. Its approximating function can be given in the following form:

$$\phi_{\mathrm{p}}(z) = \sum_{j=1}^{N} \tilde{A}_j z^j,$$
$$\psi_{\mathrm{p}}(z) = \sum_{j=1}^{N} \tilde{B}_j z^j, \tag{21}$$

where $\tilde{A}_j$ and $\tilde{B}_j$ are unknown complex constants. $\tilde{A}_1$ is a real constant because its image part has no contribution to stress. In Eq. (21), no terms corresponding to negative order of z and no constant terms are included because negative order terms give singular value of displacement, while the constant terms have no contribution to stress. The primary part induces stress at the location of the elliptic-hole edge as $\sigma_{nn} + \mathrm{i}\sigma_{nt}$.

The complementary potential functions, $-(\sigma_{nn} + \mathrm{i}\sigma_{nt})$, correspond to the prescribed traction along the boundary of the elliptic hole of the element under consideration. Thus, the complementary part is related to $\tilde{A}_j$ and $\tilde{B}_j$ only, and superposition of the two parts will satisfy the traction-free condition along the hole boundary.

To formulate the complementary potential functions, the mapping function shown in Eq. (22) is used, which maps the element in the z-plane onto exterior of an unit circle in the ζ-plane shown in Fig. 3

$$z = \omega(\zeta) \equiv E_0\zeta + E_1/\zeta, \quad E_0 = (a+b)/2, \quad E_1 = (a-b)/2, \tag{22}$$

where a and b denote semi-axes of the ellipse.

On the ζ-plane, stresses are expressed as

$$\sigma_{xx} + \sigma_{yy} = 4\mathrm{Re}\left[\frac{\varphi'(\zeta)}{\omega'(\zeta)}\right],$$
$$\sigma_{yy} - \sigma_{xx} + 2\mathrm{i}\sigma_{xy} = \frac{2}{\omega'(\zeta)}\left[\overline{\omega(\zeta)}\left\{\frac{\varphi'(\zeta)}{\omega'(\zeta)}\right\}' + \psi'(\zeta)\right]. \tag{23}$$

The traction-free boundary condition along the unit circle is expressed as

$$\varphi(\sigma) + \frac{\omega(\sigma)}{\overline{\omega'(\sigma)}}\overline{\varphi'(\sigma)} + \overline{\psi(\sigma)} = 0. \tag{24}$$

On the ζ-plane, the potential functions are still given in two parts

$$\phi(\zeta) = \phi_{\mathrm{p}}(\zeta) + \phi_{\mathrm{c}}(\zeta),$$
$$\psi(\zeta) = \psi_{\mathrm{p}}(\zeta) + \psi_{\mathrm{c}}(\zeta) \tag{25}$$

in which the primary functions are rewritten in term of another set of unknown complex constants, A_j and B_j, which is linearly related with $\tilde{A}_j$ and $\tilde{B}_j$

$$\phi_{\mathrm{p}}(\zeta) = \sum_{j=1}^{N} A_j[(E_0\zeta)^j + (E_1/\zeta)^j],$$
$$\psi_{\mathrm{p}}(\zeta) = \sum_{j=1}^{N} B_j[(E_0\zeta)^j + (E_1/\zeta)^j], \tag{26}$$

where N is the number of series terms; A_j and B_j make up the generalized co-ordinates as

$$\beta = [A_1^{\mathrm{r}}, A_2^{\mathrm{r}}, \ldots, A_N^{\mathrm{r}}, A_2^{\mathrm{i}}, A_3^{\mathrm{i}}, \ldots A_N^{\mathrm{i}}, B_1^{\mathrm{r}}, B_2^{\mathrm{r}}, \ldots, B_N^{\mathrm{r}}, \times B_1^{\mathrm{i}}, B_2^{\mathrm{i}}, \ldots B_N^{\mathrm{i}}]^{\mathrm{T}} \tag{27}$$

where A_j^{r}, A_j^{i}, B_j^{r} and B_j^{i} are the real and imaginary part of A_j and B_j, respectively.

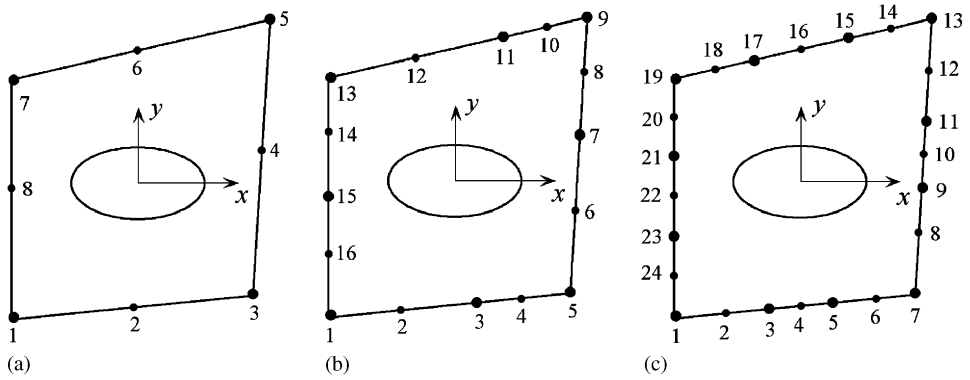

Fig. 4. Family of hybrid elements; (a) eight-node element, (b) 16-node element, (c) 24-node element.

In general, trial functions provide more accurate solutions when the series terms N (in (26)) is increased. However, as found in [4], the solutions have become unstable when more terms were selected. Decomposing the trial functions into two parts as in (25) is shown to make the solution stable with the increase in series terms in this paper (see Section 3).

For the complementary functions corresponding to each generalized co-ordinate, we try to find out a solution satisfying the traction boundary condition $-(\sigma_{nn}+\mathrm{i}\sigma_{nt})$ along the unit circle. The complementary functions corresponding to each generalized co-ordinate are not required to satisfy the displacement boundary condition along the external boundary because the displacement boundary condition can be satisfied by superposition of solutions of all the generalized co-ordinates. Thus, we assume the two complementary potential functions are analytic functions in the exterior of the unit circle. A substitution of Eqs. (24) and (25) into Eq. (23) yields

$$\varphi_{\mathrm{p}}(\sigma)+\varphi_{\mathrm{c}}(\sigma)+\frac{\omega(\sigma)}{\overline{\omega}'(\sigma)}[\overline{\varphi'_{\mathrm{p}}(\sigma)}+\overline{\varphi'_{\mathrm{c}}(\sigma)}]+\overline{\psi_{\mathrm{p}}(\sigma)}+\overline{\psi_{\mathrm{c}}(\sigma)}=0. \tag{28}$$

Multiplying both sides of Eq. (28) by $\mathrm{d}\sigma/[2\pi\mathrm{i}(\sigma-\zeta)]$ and carrying out all the Cauchy integrals along the unit circle, $\varphi_{\mathrm{c}}(\zeta)$ is derived as

$$\begin{aligned}\varphi_{\mathrm{c}}(\zeta)=&-\sum_{j=1}^{N}A_j\left(\frac{E_1}{\zeta}\right)^j-\sum_{j=1}^{N}\overline{B}_j\left(\frac{E_0}{\zeta}\right)^j+\frac{\omega(\zeta)\sum_{j=3}^{N}\overline{A}_j j\left(\frac{E_0}{\zeta}\right)^j+\frac{E_1}{E_0}[\overline{A}_1(E_0/\zeta)^2+2\overline{A}_2(E_0/\zeta)^3]}{E_1\zeta-E_0/\zeta}\\&+\frac{[1+(E_1/E_0)^2]\sum_{j=3}^{N}\overline{A}_j jE_0^j\left(\frac{E_1}{E_0}\right)^{(j-3)/2}+E_1(\overline{A}_1+2\overline{A}_2\sqrt{E_0E_1})}{2(\sqrt{E_0/E_1}-\zeta)}\\&+\frac{[1+(E_1/E_0)^2]\sum_{j=3}^{N}\overline{A}_j j(-1)^jE_0^j\left(\frac{E_1}{E_0}\right)^{(j-3)/2}-E_1(\overline{A}_1-2\overline{A}_2\sqrt{E_0E_1})}{2(\sqrt{E_0/E_1}+\zeta)}.\end{aligned} \tag{29}$$

All the terms in (29) are analytic functions, they give normal values of stresses and displacements along the element boundaries, which makes the methods stable for more series terms.

The complementary potential function, $\psi_{\mathrm{c}}(\zeta)$, can be derived similarly as $\varphi_{\mathrm{c}}(\zeta)$. Alternatively, the whole potential function $\psi(\zeta)$ can be directly derived by analytic continuation along the traction-free boundary from Eq. (23) as the following simple form:

$$\psi(\zeta)=-\overline{\varphi(1/\bar{\zeta})}-\frac{\overline{\omega(1/\bar{\zeta})}}{\omega'(\zeta)}\varphi'(\zeta). \tag{30}$$

Generally speaking, most of plane elements used in finite element software have displacement fields over the boundary of the element expressed in terms of polynomials; e.g. linear for edges with two nodes, quadratic for edges with three nodes, etc.

Therefore, the interpolation function matrix $\mathbf{L}$ in Eq. (11) should be assumed in such way that the displacement on the element boundaries varies linearly between any two adjacent nodes, or quadratically between a set of three constructive nodes, etc. to ensure the same displacements are obtained along the common boundary of two adjacent elements.

Six types of element were constructed as follows: eight-node, 16-node and 24-node elements with linearly varying displacement between two neighbouring nodes, and eight-node, 16-node, 24-node elements with quadratically varying displacement as shown in Fig. 4. The first three elements were constructed to match the standard three-noded triangular elements or the four-noded quadrilateral elements that exhibit linear displacements along their element boundaries. The last three elements were constructed to match the standard six-node triangular or eight-node quadrilateral elements. The elements with more nodes were formulated to enhance meshing for the simulation of bigger holes, while the elements with fewer nodes

were constructed for simulating smaller holes compared to the surrounding elements.

For the elements with linearly varying displacement, one can assume the displacement between the ith and $(i+1)$th nodes varies as

$$\tilde{\mathbf{u}} = \begin{bmatrix} 1-\eta, & 0, & \eta, & 0 \\ 0, & 1-\eta, & 0, & \eta \end{bmatrix} \begin{Bmatrix} u_i \\ v_i \\ u_{i+1} \\ v_{i+1} \end{Bmatrix} \equiv \mathbf{Lq}, \tag{31}$$

where $\eta = s/l$ in which l and s are the distance between the two nodes and the distance from the ith node, respectively.

For the elements with quadratically varying displacement, one can assume the displacement between the ith and $(i+2)$th nodes varies as

$$\tilde{\mathbf{u}} = \begin{bmatrix} (1-\eta)(1-2\eta), 0, 4\eta(1-\eta), 0, \eta(2\eta-1), 0 \\ 0, (1-\eta)(1-2\eta), 0, 4\eta(1-\eta), 0, \eta(2\eta-1) \end{bmatrix} \begin{Bmatrix} u_i \\ v_i \\ u_{i+1} \\ v_{i+1} \\ u_{i+2} \\ v_{i+2} \end{Bmatrix} \equiv \mathbf{Lq}, \tag{32}$$

where $\eta = s/l$ in which l and s are the distance between the ith and the $(i+2)$th nodes and the distance from the ith node, respectively. $i = 1, 3, 5, 7$ for the eight-node element, $i = 1, 3, 5, 7, 9, 11, 13, 15$ for the 16-node element, and $i = 1, 3, 5, \ldots, 23$ for the 24-node elements.

3. Validation of the hybrid-Trefftz element

With a view to validating the element formulated in Section 2, a single element subjected to uniform elongation of a prescribed value was considered. Fig. 5 shows a square element of size $2w_e$ ($w_e = 0.7$ mm) containing an elliptic hole of major axis diameter $2a$ ($a = 0.07$ mm) and minor axis diameter $2b$ ($b = 0.5a$) subjected to a vertical elongation $v = 0.5 \times 10^{-4}$ mm. The maximum size of the elliptic hole was only 10% of the size of the element in this problem. The material properties were assigned as $E = 200$ GPa, and $v = 0.3$.

The hoop stress at point P on the major axis (Fig. 5) was calculated. Several trial solutions were obtained by assuming various values for N (shown in filled circle in Fig. 6) in Eq. (29). The result exhibited some oscillation for N values below 12 (see the line with dots shown in Fig. 6); with further increase in values of N, stable solutions were obtained. The problem was also solved using the formulation provided by Piltner [4]. The results are shown as line with starts in Fig. 6. It can be seen that this method has provided unstable solution for N values greater than or equal to 14.

To examine the effect of ratio a/w_e (see Fig. 5) on the performance of the special element, the above problem was solved by setting $a = 0.35$ mm (which is 50% of the size of the element); all other parameters were kept the same as the above problem. The problem was also solved using Piltner method [4]. The variation of the hoop stress at point P with the increase in the value of N is shown in Fig. 7.

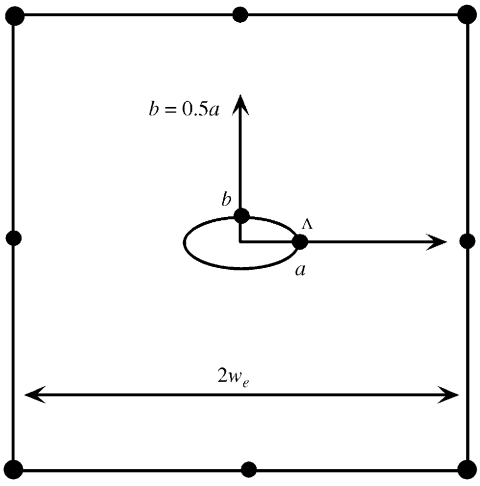

Fig. 5. An eight-noded hybrid element containing elliptic hole subjected to uniform elongation.

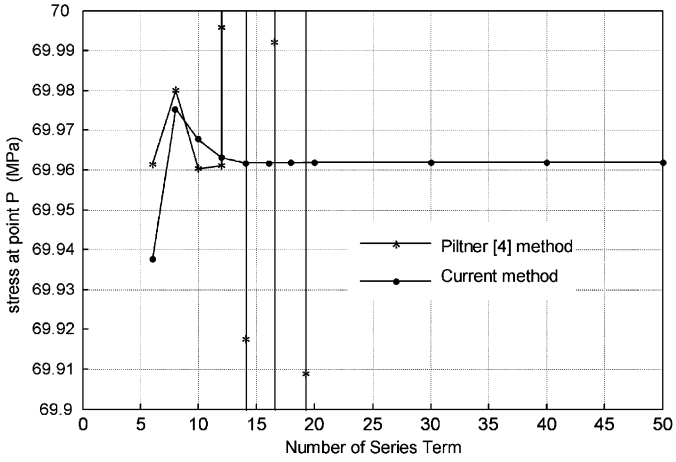

Fig. 6. Convergence of vertical stress at A with the increase in value of N (relative size of hole to element size = 10%).

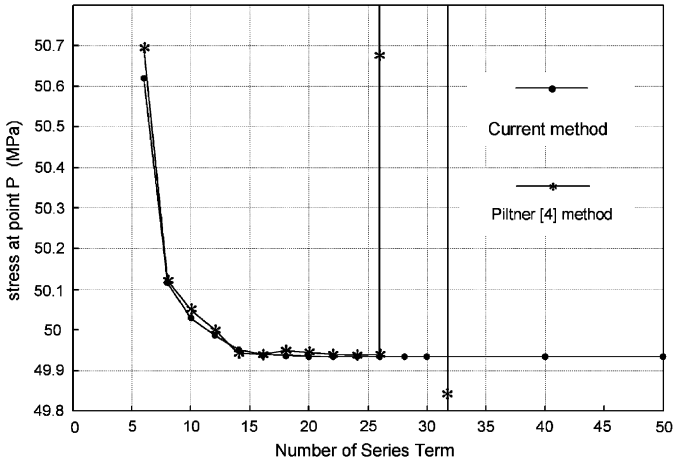

Fig. 7. Convergence of vertical stress at A with the increase in value of N (relative size of hole to element size = 50%).

Once again it can be seen that Piltner's [4] formulation became unstable for values of N more than 27 whilst the result was generally exhibiting stable convergence pattern with the increase in value of N for the element presented in this paper.

The stable convergence of the results presented in this section could be regarded validating the formulation to a limited extent. Convergence tests similar to that provided by Karihaloo and Xiao [2] were carried out to further validate the formulation but not presented here to conserve space and to illustrate the application of the element to more complex problems.

4. Application of the hybrid Trefftz to classical problems of elasticity

In this section, four numerical examples are presented to show the accuracy, efficiency, and mesh dependency of the element formulated in Section 2. The first example deals with an infinite plate containing a crack solved by Piltner [4]. The second example presents the accuracy of the proposed elements using the analytic solution for a problem of an infinite plate containing an elliptic hole subjected to a far-field uniform tension. In the third example a rectangular plate containing elliptic hole was analysed, and the results are compared with that provided by the conventional finite elements in ABAQUS. In the fourth example, mesh dependency of the elliptic-hole element is discussed. The materials for all the four examples were assumed to remain elastic with the Young's modulus of 200 GPa and Poisson's ratio of 0.3.

4.1. Example #1

The first numerical example considers the problem presented by Piltner [4]. An internal crack of 4 mm long at the centre of a square plate of size 100 mm subjected to uniform vertical uniaxial tensile loading P ($P=1$). The exact value of the Mode I SIF of the crack for this problem is 1.4142. The result reported by Piltner [4] is 1.4164.

A finite element mesh same as that generated by Piltner [4] was employed to calculate SIF of the crack as shown in Fig. 8. The 16-node element with quadratic displacements (with the number of series terms $N=15$) was used in the modelling. The problem was also solved by the method provided by Piltner [4]; in this case the number of series terms were chosen as 15 and 4 (to illustrate the effect of these choices).

The SIF for the right crack-tip was calculated from

$$K_{\mathrm{I}} - \mathrm{i}K_{\mathrm{II}} = \frac{2\varphi_{\mathrm{c}}'(\zeta)_{\zeta=1}}{\sqrt{a}}. \tag{33}$$

The SIF calculated from all these analyses is shown in Table 1. The calculations were repeated by modifying the crack length as 0.4 mm (by keeping all other parameters the same) and the results are also presented in Table 1.

It can be seen from the results shown in Table 1 that the current element provides accurate results that conform to the analytical solutions well. Piltner [4] method also predicted the SIF fairly well when the number of series terms was chosen appropriately. However, if the rule given in Piltner [4] was used for the selection of the number of terms based on the number of nodes of the element (in this case for an eight-node element, the terms required was 15), unacceptable results were predicted (both for K_{I} and K_{II}).

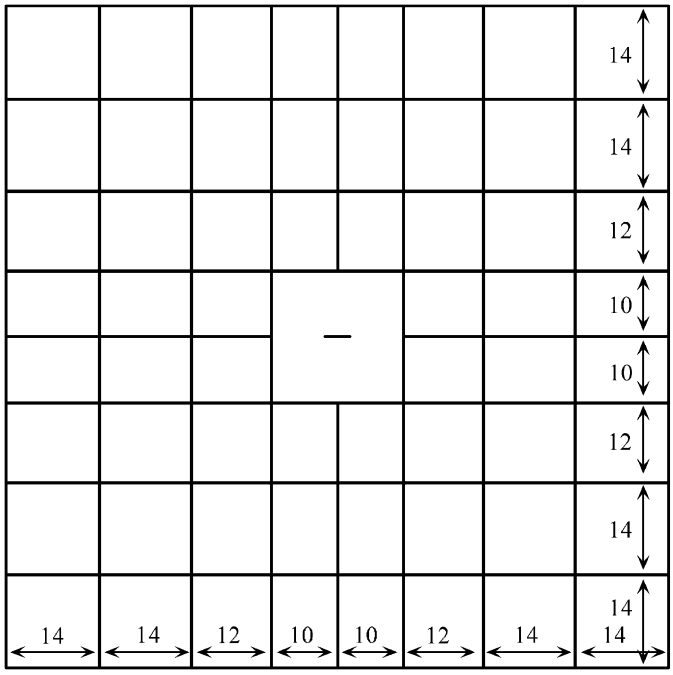

Fig. 8. Mesh for the internal crack element.

Table 1
SIF at the tip of a crack in a square plate

Crack length (mm)	Current element ($N=15$)		Piltner [4] element ($N=4$)		Piltner [4] element ($N=15$)	
	K_{I}	K_{II}	K_{I}	K_{II}	K_{I}	K_{II}
4.0	1.4141	0.0000	1.4163	0.0000	2.4855	0.0288
0.4	0.4465	0.0000	0.4471	0.0000	1.2099	0.0014

4.2. Example #2

In the second example as shown in Fig. 9, a large square plate with an elliptic hole is subjected to remote uniform tensile stress σ_0. The ratio between the semi-axis of the elliptic hole and the width of the plate was set as $a/w = 0.05$. The ratio between the two semi-axes was set as $a/b=2$. The mesh for the hybrid element calculation is shown in Fig. 9 in which one quadratic eight-node hybrid element has been used. Together with the analytic solution, the normalised stress along the edge of the hole from point A to point B is plotted against the normalised hole boundary length in Fig. 10 (l_0 is the full circumferential length of the elliptic hole). From the figure it can be seen that the element formulated in this paper produces accurate results.

The hoop stress concentrations at point A are also considered for different ratios of b/a as listed in Table 2. It can be seen from Table 2 that the current element produces accurate results for all the ratios of b/a as the errors remained below 5%.

4.3. Example #3

The third example considered a rectangular plate (width w and length $2w$) with an elliptic hole at its centre subjected to uniform tension along the vertical direction. The ratio of a/w was set as $\frac{1}{8}$. The inclination angle of the elliptic hole to the horizontal axis was defined as α. Fig. 11 shows the meshes for the current element and that used in ABAQUS simulation. The linear 16-node hybrid-Trefftz element was used. The stress concentration coefficients at points A and B were calculated from

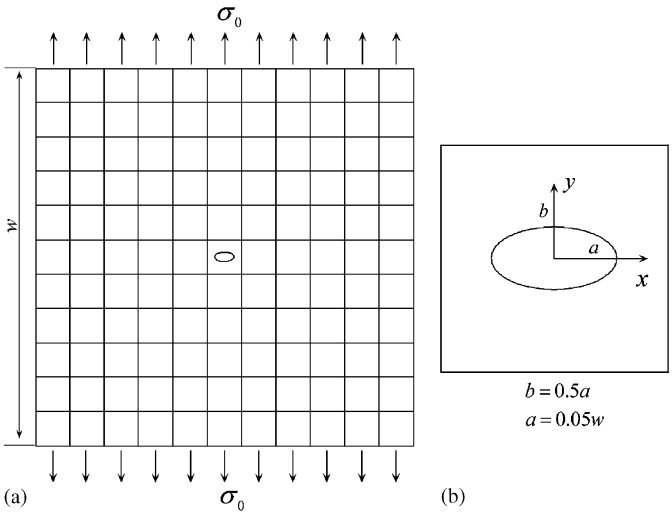

Fig. 9. A large square plate subjected to tension; (a) mesh for current element, (b) the current element.

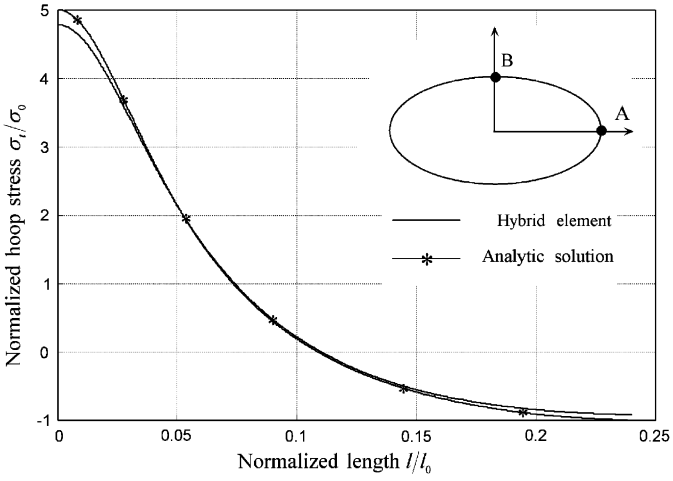

Fig. 10. Normalised hoop stress varies against normalised length.

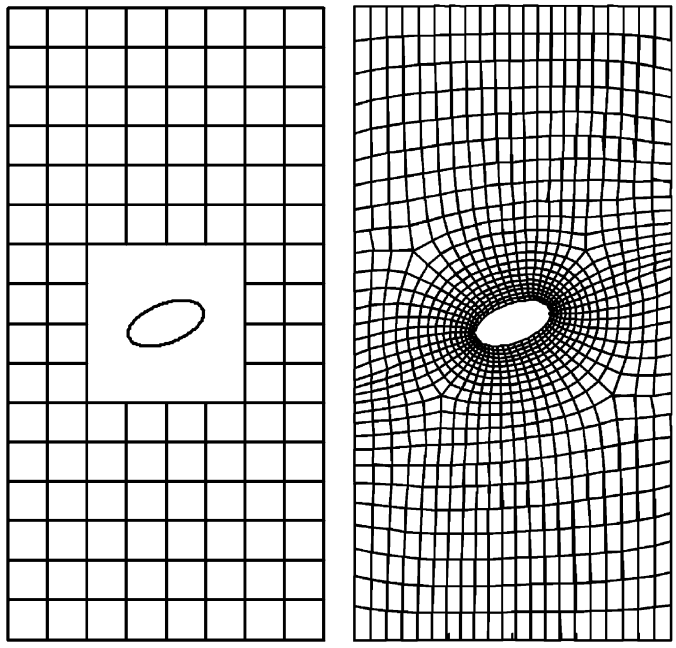

Fig. 11. Meshes for hybrid element and the elliptic hole; (a) mesh for current element, (b) mesh for conventional finite element.

both analyses and presented in Fig. 12 as a function of the inclination angle α. From Fig. 12 it can be seen that the two results agree very well with each other. The good coincidence demonstrates the accuracy of the current element. However, as shown in Fig. 11, the mesh is much simpler when the current element has been used. Furthermore, when the inclination angle of the elliptic hole was changed, the mesh for the current element was not changed at all—thus saving much time and effort in modelling compared to conventional finite element modelling.

4.4. Example #4

Although the special hybrid element presented in this paper offers much convenience in meshing, one still has to take care in not violating certain norms of modelling—in particular, the ratio a/w_e in which a is the major semi-axis of the elliptic hole and w_e is the width of the element (assuming a and w_e are located along the same axis). To examine the norm, the problem presented in example #1 was re-analysed; the elliptic hole size a was kept constant whilst the element size w_e was varied. The elliptic hole was located at the centre of the element and its axis was kept parallel to the square edge of the element. A square eight-node element was used in the analysis.

Table 2
Hoop stress concentration for different ratios of b/a

b/a	1.0	0.9	0.8	0.7	0.6	0.5	0.4	0.3	0.2	0.1	0.05	0.01
Analytic	3	3.22	3.50	3.86	4.33	5.00	6.00	7.67	11	21	41	201
Current	2.87	3.07	3.33	3.67	4.13	4.78	5.75	7.38	10.62	20.37	39.82	195.6
Error (%)	4	5	5	5	5	4	4	4	3	3	3	3

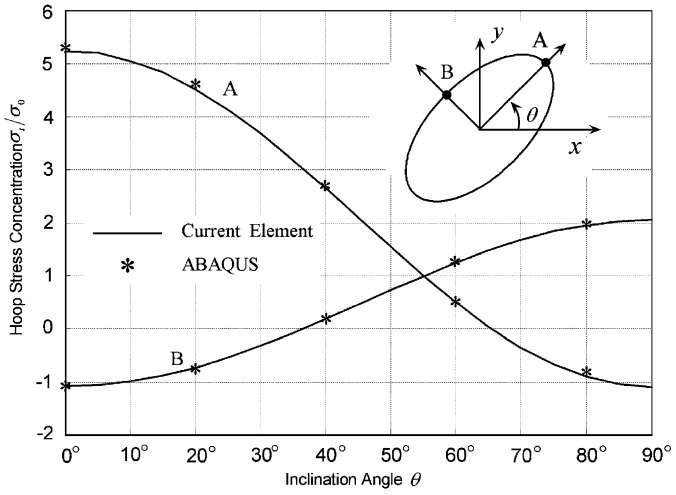

Fig. 12. Variation of hoop stress concentrations due to the inclination angle θ.

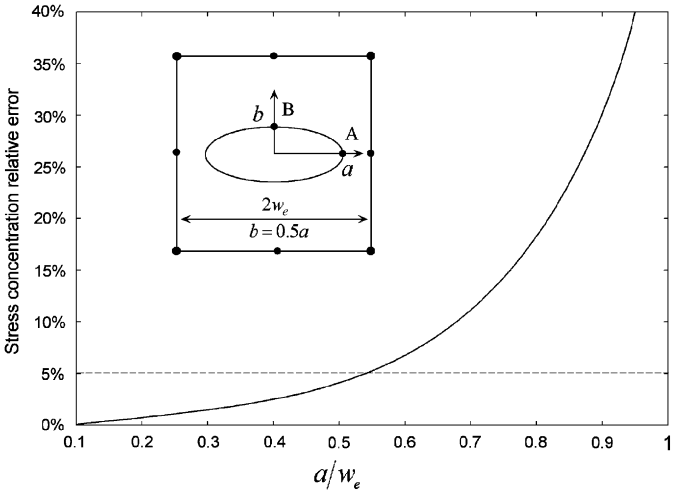

Fig. 13. Variation of relative error in hoop stress concentration against the ratio a/w_e.

This classical problem has an analytical solution of the highest stress concentration at point A, whose value is 5. Incidentally point A suffers from maximum possible error in the calculated hoop stress, as this point is the closest to the sides of the hybrid-Trefftz element. Thus, we use the hoop stress concentration at point A to check the element size sensitivity. Ten different size ratios of a/w_e were considered for the hybrid-Trefftz element. The stress concentration coefficients at point A are shown in Fig. 13. It can clearly be seen that the size of the current element (relative to the size of the elliptic hole) influences the result. For the problem considered, it can be concluded that as long as the ratio a/w_e is kept lower than 0.5, the error in stress concentration factor will remain below 5%. Obviously, when modelling a hole of a defined size, it is prudent to choose the size of the hybrid-Trefftz element at least twice as that of the size of the hole.

It is worthy to note that for accurate results, when the current element is used to simulate bigger size holes, the hybrid element size should be of at least twice of their size, to keep the size ratio a/w_e as small as possible. If all elements (ordinary finite elements) are kept the same size of the current element, accuracy of the solution would be adversely affected; this requires small size ordinary elements surrounding a big size hybrid-Trefftz element. Adding more nodes to the sides of the hybrid-Trefftz element meets both of these conflicting requirements.

5. Application of the hybrid-Trefftz element to bending problems

A simply supported rectangular steel plate ($E=200$ GPa and $v=0.3$) of depth $=200$ mm, span$=400$ mm, thickness$=15$ mm, containing four circular holes of diameter 30 mm each subjected to four point bending (Fig. 14) was analysed using the

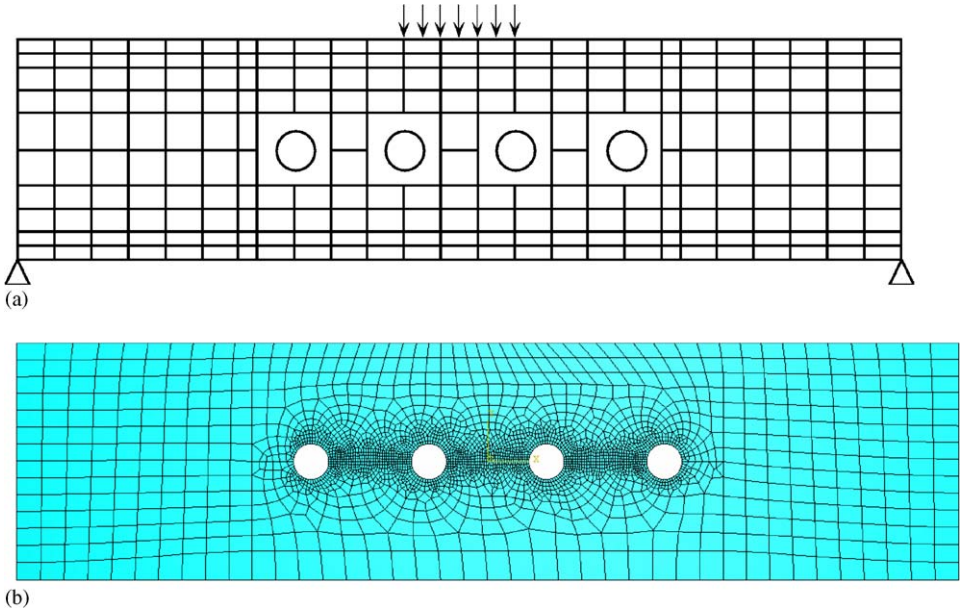

Fig. 14. Meshing schemes for four-holed rectangular plate subjected to bending: (a) mesh using square 16-node hybrid-Trefftz element; (b) mesh using quadratic conventional finite elements.

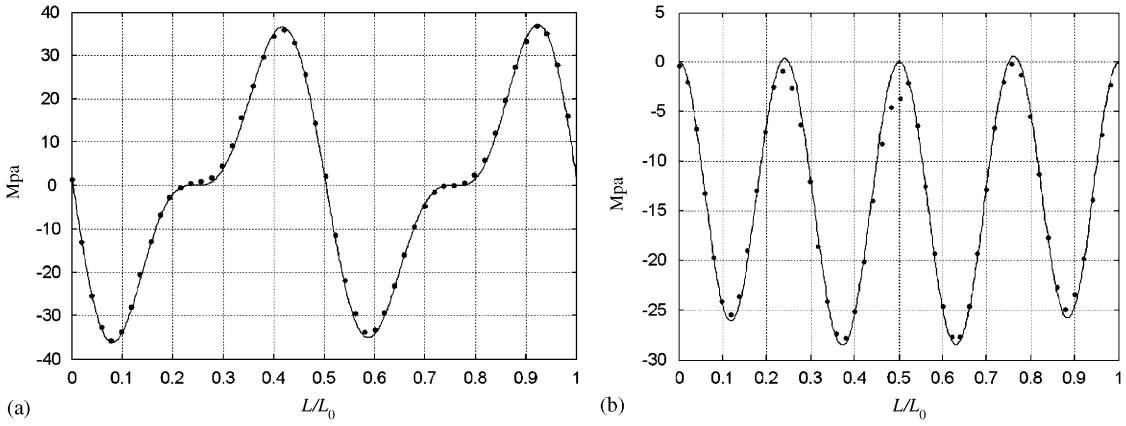

Fig. 15. Stress state around the hole.

hybrid-Trefftz element presented in this paper and the conventional finite element method. The mesh shown in Fig. 14a was used for the analysis using current element and the mesh shown in Fig. 14b was used for the analysis using conventional finite element method.

The hoop stress and inplane shear stress around one of the holes adjacent to the vertical axis of symmetry is plotted as a function of the normalised circumferential length of that hole in Fig. 15. The results obtained from the conventional finite element (ABAQUS) FE solution are also shown in this figure.

It can be seen from Fig. 15 that the results predicted by the current method in spite of using coarser mesh has provided good result which agree well with the ABAQUS prediction.

6. Conclusions

A family of hybrid-Trefftz elements containing elliptic hole has been formulated using the complex variable technique and the Hellinger–Reissner variational principle in this paper. The elements have different number of nodes which lead to linearly and quadratically varying displacement functions along their boundary to match with different surrounding standard finite elements.

Through considering a series of numerical examples it has been shown that the current element can be considered as an improvement over the element presented by Piltner [4]; and can predict SIF and stress concentration factors effectively by using relatively coarse meshes. It has also been shown that the hybrid-Trefftz element should be at least twice as large as the size of the embedded hole for accurate determination of stress concentration factor.

Acknowledgement

The RAAS 2003 Grants Scheme of the Central Queensland University funded this project.

References

[1] P. Tong, T.T.H. Pian, S.L. Lasy, A hybrid-element approach to crack problems in plane elasticity, Int. J. Numer. Methods Eng. 7 (1973) 297–308.
[2] B.L. Karihaloo, Q.Z. Xiao, Accurate determination of the coefficients of elastic crack tip asymptotic field by a hybrid crack element with *p*-adaptivity, Int. J. Eng. Fracture Mech. 68 (2001) 1609–1630.
[3] D. Zeng, N. Katsube, J. Zhang, W. Soboyejo, Hybrid crack-tip element and its application, Finite Elements Anal. Design 38 (2002) 319–335.
[4] R. Piltner, Special finite elements with holes and internal cracks, Int. J. Numer. Methods Eng. 21 (1985) 1471–1485.
[5] R. Piltner, Comments on Development of two dimensional elements with a central circular hole, Comput. Methods Appl. Mech. Eng. 191 (2001) 503–504.
[6] R. Piltner, Recent developments in the Trefftz method for finite element and boundary element applications, Adv. Eng. Software 24 (1995) 107–115.
[7] J.A. Teixeira, Z.Y. Ji, Hybrid-Trefftz finite element formulation for simulation of singular stress fields, Int. J. Numer. Methods Eng. 39 (1996) 281–308.
[8] J.A. Teixeira, Z.Y. Ji, Hybrid-Trefftz equilibrium model for crack problems, Int. J. Numer. Methods Eng. 39 (1996) 569–584.
[9] Q.H. Qin, The Trefftz Finite and Boundary Element Method, Southamptom, WIT Press, UK, 2000.
[10] J. Zhang, N. Kastsube, Hybrid finite element method for heterogeneous materials with randomly dispersed rigid inclusions, Int. J. Numer. Methods Eng. 38 (1995) 1635–1647.
[11] J. Zhang, N. Kastsube, Hybrid finite element method for heterogeneous materials with randomly dispersed elastic inclusions, Finite Elements Anal. Design 19 (1995) 45–55.
[12] Z.S. Tian, J.S. Liu, B. Fang, Stress analysis of solids with rectangular holes by 3D special hybrid stress elements, Struct. Eng. Mech. 3 (1995) 193–199.
[13] J.A. Kolodziej, A. Uscilowska, Trefftz-type procedure for Laplace equation on domains with circular holes, circular includions, corners, slits and symmetry, Comput. Assisted Mech. Eng. Sci. 4 (1997) 501–519.
[14] O.C. Zienkiewicz, Trefftz type of approximation and the finite element method—history and development, Comput. Assisted Mech. Eng. Sci. 4 (1997) 305–316.
[15] J.A.T. Freitas, Z.Y. Ji, Hybrid-trefftz equilibrium model for crack problems, Int. J. Number Methods Eng. 39 (1996) 569–584.
[16] N.I. Muskhelishvili, Some Basic Problems of Mathematical Theory of Elasticity, fourth ed., Noordhoff, The Netherlands, 1963.